Heliyon 10 (2024) e34337

Contents lists available at ScienceDirect

Heliyon

journal homepage: www.cell.com/heliyon

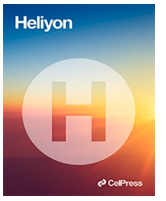

Research article

Plasma-activated water: Candidate hand disinfectant for SARS-CoV-2 transmission disruption

Yong Xu [a,1], Tao Jin [b,1], Yu Bai [a], Xiuhong Zhou [a], Han Lv [a], Chenwei Dai [a,***], Zhengwei Wu [b,**], Qinghua Xu [a,c,*]

[a] Anhui Academy of Medical Sciences, Anhui Medical College, Hefei, China
[b] School of Nuclear Science and Technology, University of Science and Technology of China, Hefei, China
[c] Anhui Provincial Center for Disease Control and Prevention, Hefei, China

ARTICLE INFO

Keywords:
Plasma-activated water
SARS-COV-2
Swine skin
Hand disinfectant

ABSTRACT

The global epidemic caused by SARS-CoV-2 has brought about worldwide burden and a sense of danger for more than two years, leading to a wide range of social, public health, economic and environmental issues. Self-inoculation through hands has been the primary way for environmental transmission of SARS-CoV-2. Plasma-activated water (PAW) has been reported as an effective, safe and environmentally friendly disinfectant against SARS-CoV-2. However, the inactivating effect of PAW on SARS-CoV-2 located on skin surface and its underlying mechanism of action have not been elucidated. In this study, PAW was prepared using an air-pressure plasma jet device. The antiviral efficiency of PAW1, PAW3, and PAW5 on the SARS-CoV-2 pseudovirus was 8.20 % (±2.88 %), 46.24 % (±1.79 %), and 91.71 % (±0.47 %), respectively. Additionally, determination of PAW's physicochemical properties, identification of major sterile effector in PAW, transmission electron microscopy analysis, malondialdehyde (MDA) assessment, SDS-PAGE, ELISA, and qPCR were conducted to reveal the virucidal mechanism of PAW. Our experimental results suggested that peroxynitrite, which was generated by the synergism of acidic environment and reactive species, was the major sterile effector of PAW. Furthermore, we found that PAW treatment significantly inactivated SARS-CoV-2 pseudovirus through the destruction of its structure of and the degradation of the viral RNA. Therefore, the possible mechanism for the structural destruction of SARS-COV-2 by PAW is through the action of peroxynitrite generated by the synergism of acidic environment and reactive species, which might react with and destroy the lipid envelope of SARS-CoV-2 pseudovirus. Nevertheless, further studies are required to shed light on the interaction mechanism of PAW-inherent RONS and viral components, and to confirm the determinant factors for virus inactivation of SARS-COV-2 by PAW. Therefore, PAW may be a candidate hand disinfectant used to disrupt the transmission of SARS-CoV-2.

* Corresponding author. Anhui Academy of Medical Sciences, Anhui Medical College, Hefei, China.
** Corresponding author. University of Science and Technology of China, Hefei, China.
*** Corresponding author. No.15 Gongwan road, Hefei city, Anhui province, China.
E-mail addresses: daichenwei_123@163.com (C. Dai), wuzw@ustc.edu.cn (Z. Wu), xqh1126@sina.com (Q. Xu).
[1] Y.X. and T.J. contributed equally to this paper.

https://doi.org/10.1016/j.heliyon.2024.e34337
Received 21 March 2024; Received in revised form 19 June 2024; Accepted 8 July 2024
Available online 9 July 2024

1. Introduction

The global pandemic of coronavirus disease 2019 (COVID-19) has resulted in significant social, public health, economic, and environmental challenges [1]. Severe acute respiratory syndrome coronavirus 2 (SARS-CoV-2), the causative agent of COVID-19, primarilys alveolar epithelial cells, leading to respiratory tract transmission [2]. The genome of SARS-CoV-2 consists of a single-stranded positive-sense RNA (+ssRNA) surrounded by a capsid formed by the nucleocapsid protein (N protein). The capsid is enveloped by a lipid membrane composed of the membrane protein (M protein), spike glycoprotein (S-protein), and envelope protein (E protein) [3]. The S-protein, located on the surface of the lipid envelope, plays a crucial role in binding to the receptor angiotensin-converting enzyme 2 (ACE2) and mediating viral entry into host cells [3,4]. The receptor-binding domain (RBD), with an approximate size of 34 kDa, is an important region of S1 which specifically binds to the receptor angiotensin-converting enzyme 2 (ACE2) mediating the entry of SARS-CoV-2 into the host cells [4].

In addition to respiratory droplets, SARS-CoV-2 has been detected on various surfaces commonly touched by hands, such as stainless steel, plastics, and paper currency [5]. Self-inoculation, where contaminated hands come into contact with mucosal regions of the face, is a significant mode of transmission [6]. Self-inoculation is a form of contact transmission, where a person's contaminated hands contact with the mouth, eyes, and nostrils, introducing the pathogens to oneself via an mucosal region [6,7]. SARS-CoV-2 remains highly infectious on the skin surface, even for extended periods [5b]. Therefore, hand hygiene is of utmost importance in preventing the environmental spread of SARS-CoV-2 [5b,8].

Cold atmospheric plasma (CAP) is obtained at ambient temperature and atmospheric pressure, and contains great quantities of reactive oxygen species (ROS) and reactive nitrogen species (RNS), such as hydroxyl radicals (•OH), singlet oxygen ($^1O_2$), nitrogen dioxide (NO_2), nitric oxide (NO), and ozone (O_3) [9]. Based on their discharge mode, the most commonly used CAP devices can be divided into dielectric barrier discharge (DBD), air-pressure plasma jet (APPJ), and corona discharge devices [9b].

CAP has been proposed as a potential technology for the disinfection of surfaces contaminated by various pathogens [10]. For instance, Chen et al. observed that Ar-fed CAP jet treatment for 3 min inactivated 100 % of SARS-CoV-2 on plastic, metal, cardboard, basketball composite leather, football leather, and baseball leather [11]. In our previous study, we reported that air-DBD treatment exerted dose-dependent inactivating effect on SARS-CoV-2 on stainless steel surface [12].

Plasma-activated water (PAW) is produced by treating water with CAP, resulting in the generation of reactive species that possess antimicrobial properties [13]. PAW has been shown to effectively inactivate a wide range of microorganisms, including bacteriophages and viruses, making it a promising disinfectant [14]. When the reactive species of CAP are dissolved in water, the generated long-living secondary reactive species, such as H_2O_2 (hydrogen peroxide), NO_3^- (nitrate), and NO_2^- (nitrite) anions, are effective in inhibiting microorganism growth [15]. PAW-inherent ROS and RNS (RONS) damaged both the nucleic acids and proteins of bacteriophages T4, 174, MS2, and Newcastle disease virus, causing their inactivation [16]. Guo et al. found that PAW effectively inactivated SARS-CoV-2 pseudovirus in solution through modification on the RBD of its spike protein [17]. Compared with traditional chemical sanitizers, such as chlorinated disinfectants, 75 % ethanol and iodophor, PAW is more easily prepared, more environmentally friendly, and less toxic [13,18]. Therefore, PAW exhibits great potential as an effective, safe, and green hand disinfectant that can minimize the environmental transmission of SARS-CoV-2.

Compared with object surfaces, the structure of human skin is more complex, which contains plenty of substances, such as urea, lipids, and inorganic salts. When the skin is contaminated, pathogens can be found not only on the surface of the skin, but also in the deeper areas of the stratum corneum or in the hair follicles [19]. Lademann et al. reported that CAP treatment reduced by 94 % the bacterial contamination on swine skin [20]. On chicken skin, PAW showed 0.35 log CFU/mL of *E. coli* and 0.73 log CFU/mL of *S. aureus* decrement, respectively [21]. However, the inactivation effects of PAW on SARS-CoV-2 on the skin surface have not been reported.

In this study, we evaluated the inactivating effects of PAW on SARS-CoV-2 pseudovirus located on swine skin. We prepared PAW using an air-pressure plasma jet device and evaluated its inactivation effects using microscopy and molecular techniques. Additionally,

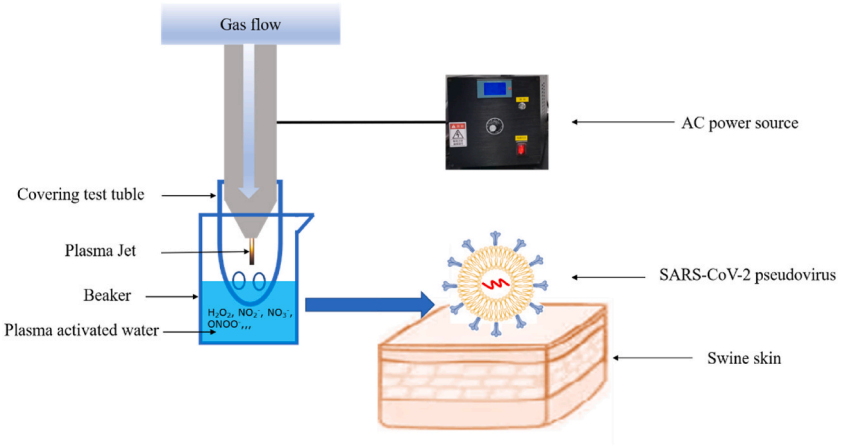

Fig. 1. Experimental process of PAW preparation and treatment against SARS-CoV-2 pseudovirus on swine skin.

we investigated the physicochemical properties of PAW and explored the possible virucidal mechanisms. Our results suggest that PAW has the potential to be used as an effective hand disinfectant to disrupt the transmission of SARS-CoV-2.

2. Materials and methods

2.1. CAP device and preparation of PAW

In this study, PAW was prepared with APPJ device (Fig. 1). This device has been designed and manufactured by ourselves, which is connected to a 140 kHz AC power source with a high voltage of 20 kV. The working gas was air at a flow rate of 40 L/min. A volume of 100 mL of PAW was prepared by CAP irradiation of ultrapure water (100 mL) in a 250-mL beaker. To avoid liquid splashing and loss, and ensure sufficient interaction between the plasma and ultrapure water, a test tube with four holes at its bottom was designed to cover the APPJ nozzle. The distance between the APPJ plume and the ultrapure water was fixed at 2 cm, and the four holes of the covering test tube were half-submerged in ultrapure water. Three groups of PAW samples were prepared under CAP irradiation for 1, 3, and 5 min, which were named PAW1, PAW3, and PAW5, respectively. The untreated ultrapure water was set as a control group (CR).

2.2. Antiviral activity assay

2.2.1. Pseudovirus treatment

Due to the high infectivity and pathogenicity of SARS-CoV-2, experiments need to be performed under high-level safety measures in biosafety level-3 (BSL-3) laboratories, which has severely limited the development of antiviral research. The pseudovirus has the ability to infect cells, similar to the true virus but without its replication ability, and thus can be safely handled in biosafety level-2 (BSL-2). Pseudovirus of SARS-CoV-2 (Fubio, China) with the SARS-CoV-2 S-protein and RNA sequence of GFP, was subjected to PAW treatments. First, swine skin without hair was obtained from a trusted local butcher. This skin was carefully excised from the upper region of the front leg of a female Landrace swine weighing between 30 and 40 kg. Following this, the skin underwent a thorough cleansing using ultrapure water and was subsequently disinfected by exposure to ultraviolet light for a duration of 30 min. Finally, the skin was precisely cut into squares measuring 0.25 × 0.25 cm. Then, 10 μL of 2×10^7 TU/mL pseudovirus solution was placed on the swine skin, air-dried for 20 min in a biosafety cabinet, and treated with 10 μL of PAW and untreated ultrapure water for 1 min. Finally, the pseudovirus was eluted from the swine skin with complete culture medium (CCM containing 89 %(v/v) Dulbecco's modified Eagle's medium (DMEM, Biological Industries, Israel), 10 %(v/v) fetal bovine serum (Excell bio, China), and 1 % (v/v) penicillin-streptomycin (Biological Industries, Israel)), to obtain 120 μL of pseudovirus-containing CCM.

2.2.2. Infection assay

The host cell, which is human embryonic kidney (HEK) 293T cell overexpressing ACE2 receptor, was purchased from Fubio (Jiangsu, China). First, HEK 293T cell were incubated in a 96-well plate at 37 °C and 5 % CO_2 until its coverage rate reached 40 %. Next, the residual CCM in each well was removed and cells were infected with 120 μL of pseudovirus-containing CCM. After incubation for 7 h, the pseudovirus-containing CCM was replaced with fresh CCM and cultured for 72 h. Finally, the pseudovirus infection was monitored using an inverted fluorescence microscope (Leica, Germany) at 100 × magnification. The number of GFP-positive spots was counted using fluorescent enzyme-linked ImmunoSpot® analyzer manufactured by Cellular Technology Ltd. (CTL, Cleveland, OH, USA).

2.3. Transmission electron microscopy

Different from the antiviral activity assay, 200 μL of phosphate buffered saline (PBS) was first used to elute the swine skin to obtain pseudovirus-containing PBS. Then, 2 μL of the pseudovirus-containing PBS was deposited on a 230-mesh copper screen and stained with 2 % uranyl acetate. Finally, the post-treatment pseudoviral morphology in the different groups was examined using a 120-kV transmission electron microscope (FEI, USA) at × 43,000 magnification.

2.4. Physicochemical properties of PAW

The pH and electrical conductivity of PAW were detected by a pH meter (Mettler-Toledo, USA) and an electrical conductivity meter (Leici, China) respectively. The ORP values were determined using an ORP electrode (Mettler-Toledo, Columbus, OH, USA), which was connected to the same pH meter. All experiments were performed in triplicate.

The H_2O_2 concentration of PAW was measured by a Hydrogen Peroxide Assay Kit (Beyotime, China) following the operation procedure manual. To quantify the NO_3^- concentration of PAW, 200 μL of 1 mol/L hydrochloric acid and 20 μL of 0.8 % sulfamic acid were added to 10 mL PAW, followed by determination through ultraviolet absorption spectrometry (Jinghua, China) at 220 nm [22]. The level of NO_2^- of PAW was determined at 540 nm using 200 μL of 10 g/L sulphanilamide as a diazotizing reagent and 200 μL of 1.0 g/L N-(1-naphthy1)-ethylenediamine hydrochloride as a coupling reagent [23].

2.5. Malondialdehyde (MDA) assessment

MDA levels were assessed using a Lipid Peroxidation MDA Assay Kit (Beyotime, China). First, 100 μL of pseudovirus-containing

PBS, which was prepared by the method described above, was added to a microfuge tube. Then, 100 μL working solution for MDA detection was added, mixed and heated for 15 min at 100 °C in a boiling water bath. After cooling to room temperature, the mixture was centrifuged at 1000×*g* for 10 min to obtain 200 μL of supernatant. Finally, the absorbance of the supernatant was measured by a microplate meter (Molecular Devices, USA) at 532 nm. To eliminate the interference of the self-contained lipid on the swine skin [24], the swine skin without SARS-CoV-2 pseudovirus was treated with the same PAW, and then the detected MDA concentration was used for MDA calibration in the treatment and control groups.

2.6. RBD protein measurement

RBD protein solution was dropped onto the swine skin, followed by treatment with CR, PAW1, PAW3, and PAW5, and five-fold elution with PBS to obtain 120 μL of RBD-containing PBS. In this study, SDS-PAGE and ELISA were applied to detect the molecular weight and antigenic changes of RBD, respectively.

In SDS-PAGE assay, electrophoresis was conducted according to the procedure described in our previous study, but the silver staining was performed instead of Coomassie bright blue staining using a Rapid Silver Staining Kit (Beyotime, China), which is more sensitive to small protein fragments.

The binding activity of the RBD protein was measured with the SARS-CoV-2 spike protein S1 RBD ELISA Kit according to the manufacturer's protocol (Elabscience, China). A volume of 20 μL of RBD-containing PBS and the biotinylated anti-RBD antibody were added onto the plate, which was simultaneously coated with an anti-RBD antibody. The absorbance value was measured at 450 nm (A_{450nm}) with a microplate meter (Bio-Rad Laboratories, Hercules, CA, USA).

2.7. Pseudoviral RNA extraction and quantitative polymerase chain reaction (qPCR)

Briefly, the Virus RNA Kit (Tiangen, China) was used to extract pseudoviral RNA, whose concentration and purity were qualified to be reversely transcribed using an ultra-micro nucleic acid protein tester (Jiapeng, China) to inspect. Reverse transcription and real-

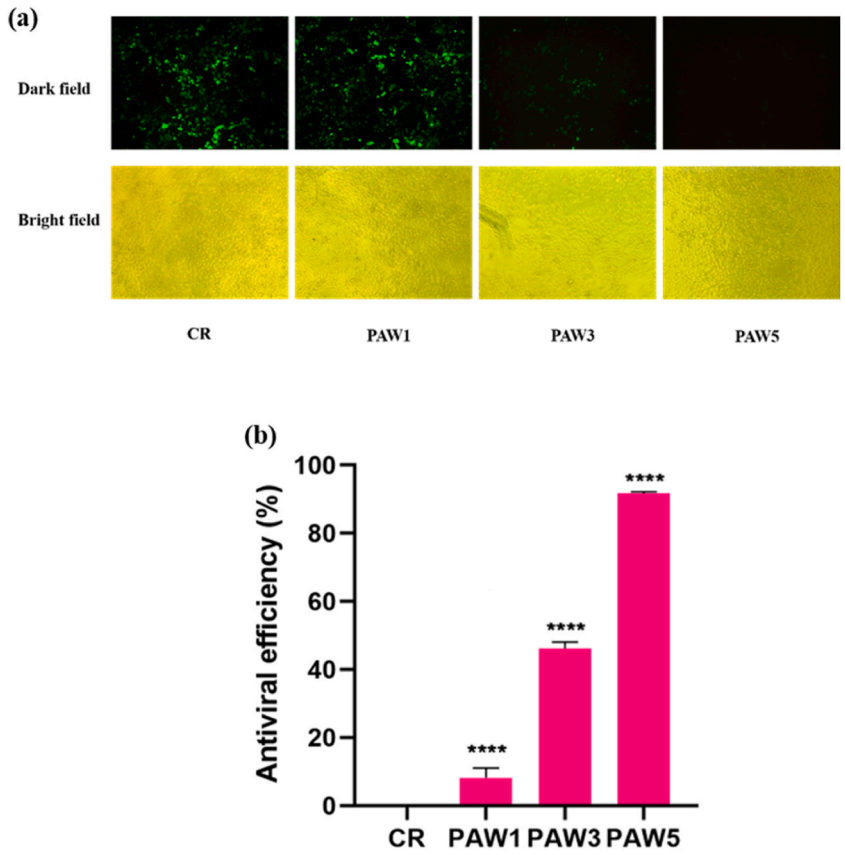

Fig. 2. Suppressive effects of CR, PAW1, PAW3, and PAW5 on the pseudovirus. a) The pseudovirus infection was monitored using an inverted fluorescence microscope. The number of the cells in the bright fields was approximately 2500. The lower number of GFP-positive cells in the dark fields indicated attenuated infection capacity of the pseudovirus treated with PAWs. Notably, the pseudovirus treated with PAW5 completely lost its infective capacity. b) The antiviral efficiency of CR and PAWs. "****" indicates extremely significant difference as compared with the CR group ($P < 0.0001$).

time PCR were conducted following the manufacturer's instructions of the cDNA First Strand Synthesis Kit (Tiangen, China) and the Fluorescent Quantitative Detection Kit (Tiangen, China), respectively. PCR was applied to detect the target sequence of luciferase (Luc) in the pseudoviral genome using Ct values. The primers of Luc, the reaction solutions and time setting were previously described. In this assay, the percentage reductions of RNA in the pseudovirus were calculated according to the formula [25]:

$$\%RNA\ reduction = \frac{\text{“}\ Treated\ Sample\ Ct\ Value\text{”} - \text{“}K\ Ct\ Value\text{”}}{40 - \text{“}K\ Ct\ Value\text{”}}$$

The upper detection limit of Ct for Luc was 40 and was approximated to 100 % of the eliminated RNA, and "K" refers to pseudovirus without PAW treatment [25].

2.8. Cytotoxicity of PAW against normal skin cells

Normal human HaCaT keratinocytes were used to evaluate the cytotoxicity of PAW. HaCaT cells was inoculated into 96-well cell culture plates at a density of 5×10^3 cells/well. After 24 h, 10 μL of PAW5 was added to each well, followed by incubation for 6 h. Cell viability was then estimated as a ratio to untreated cells. Cell Counting Kit-8 (CCK8) (Sangon, China) was used based on absorbance at 450 nm.

2.9. Statistical analysis

All experimental data are presented as mean ± standard deviation (SD) from at least three replicates. The differences between the control group and the treatment groups were subjected to one-way ANOVA and Tukey's test at a 5 % significance level. Both data analysis and charts plotting were completed using GraphPad Prism 8 (GraphPad Software Inc.; San Diego, CA, USA). The statistical significance of the differences was indicated as follows: $^{*}P < 0.05$, $^{**}P < 0.01$, $^{***}P < 0.001$, and $^{****}P < 0.0001$.

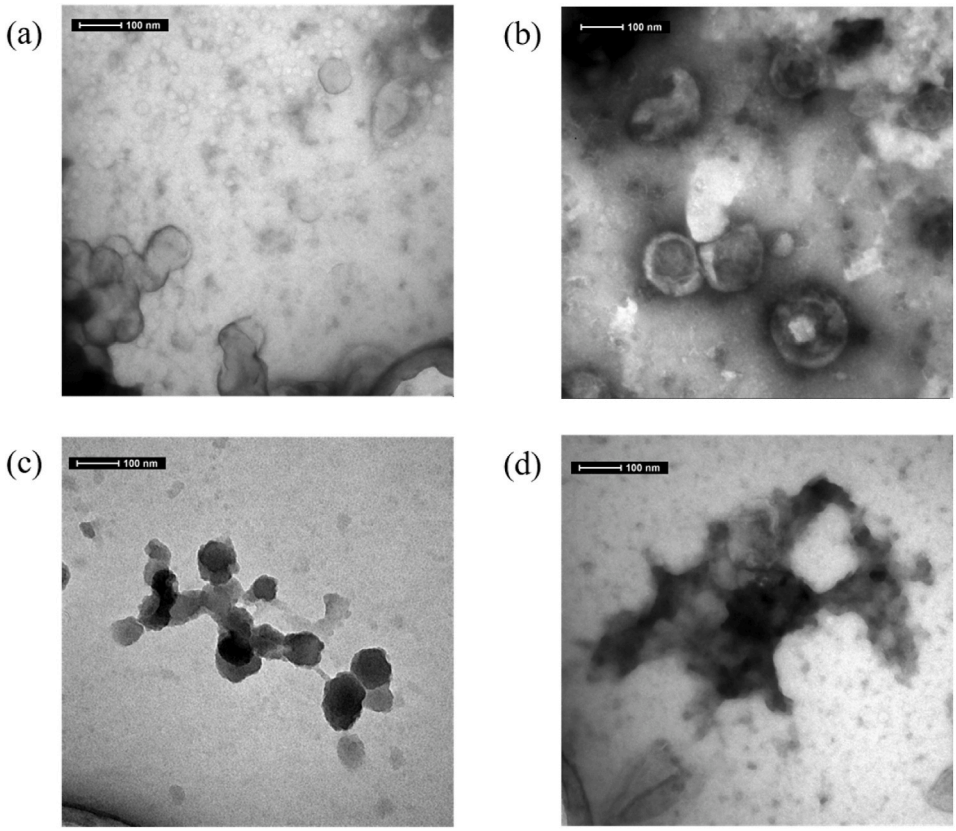

Fig. 3. Transmission electron microscopy (TEM) analysis of the pseudovirus treated with CR (a), PAW1 (b), PAW3 (c), and PAW5 (d) (plotting scale: 100 nm).

3. Results

3.1. Infective capacity of the pseudovirus

The pseudovirus used in this experiment successfully invaded 293T cells overexpressing the ACE2 receptor and expressed GFP upon successful infection. Therefore, the expression of GFP was measured to assess the infectious efficiency of the pseudovirus. The number of GFP-positive cells in a defined area containing approximately 2500 cells was determined. As shown in Fig. 2a, the number of GFP-positive cells in the pseudovirus-infected cells treated with CR and PAW1 were comparable. However, PAW3 demonstrated effective inactivation of the pseudovirus, as indicated by the significantly lower number of GFP-positive cells. Encouragingly, no GFP-positive cells were observed in the cells infected with the pseudovirus treated with PAW5. To further quantify the differences in antiviral effects between PAW1, PAW3, and PAW5, a fluorescence enzyme-linked immunospot assay was performed to count the GFP-positive cells in each well. As depicted in Fig. 2b, the numbers of GFP-positive cells in the PAW1, PAW3, and PAW5 treatments were significantly lower compared to the CR treatment. The antiviral efficiency of PAW1, PAW3, and PAW5 against the SARS-CoV-2 pseudovirus was determined to be 8.20 % (±2.88 %), 46.24 % (±1.79 %), and 91.71 % (±0.47 %), respectively.

3.2. Morphological pseudovirus changes by PAW

The morphological changes induced by PAW have been recognized as a crucial mechanism underlying its action in preventing microbial infections [26]. Therefore transmission electron microscopy (TEM) was employed to investigate the morphological alterations of the pseudovirus. Uranyl acetate staining was used to visualize the inner contents of the pseudovirus, which lacked intact structure. As depicted in Fig. 3a and b, the pseudovirus structures remained intact following treatment with CR and PAW1, with no penetration of uranyl acetate dye into the pseudovirus. However, Fig. 3© revealed that the pseudovirus treated with PAW3 was still intact, yet displayed extensive internal staining. Notably, no intact pseudovirus was observed after treatment with PAW5 (Fig. 3d). The TEM results strongly suggested that the presence of reactive oxygen and nitrogen species (RONS) in PAW led to the destruction of the viral structure.

3.3. Physicochemical properties of PAW

To establish the mechanism of PAW virucidal action, we determined its physicochemical properties, including pH, electrical conductivity, ORP, H_2O_2, and NO_3^- and NO_2^- concentration. As shown in Fig. 4a, the pH of PAW was significantly decreased to 2.86 (0.02) after 5 min of CAP irradiation. As presented in Fig. 4b and c, under CAP treatment in 5 min, the electrical conductivity and ORP

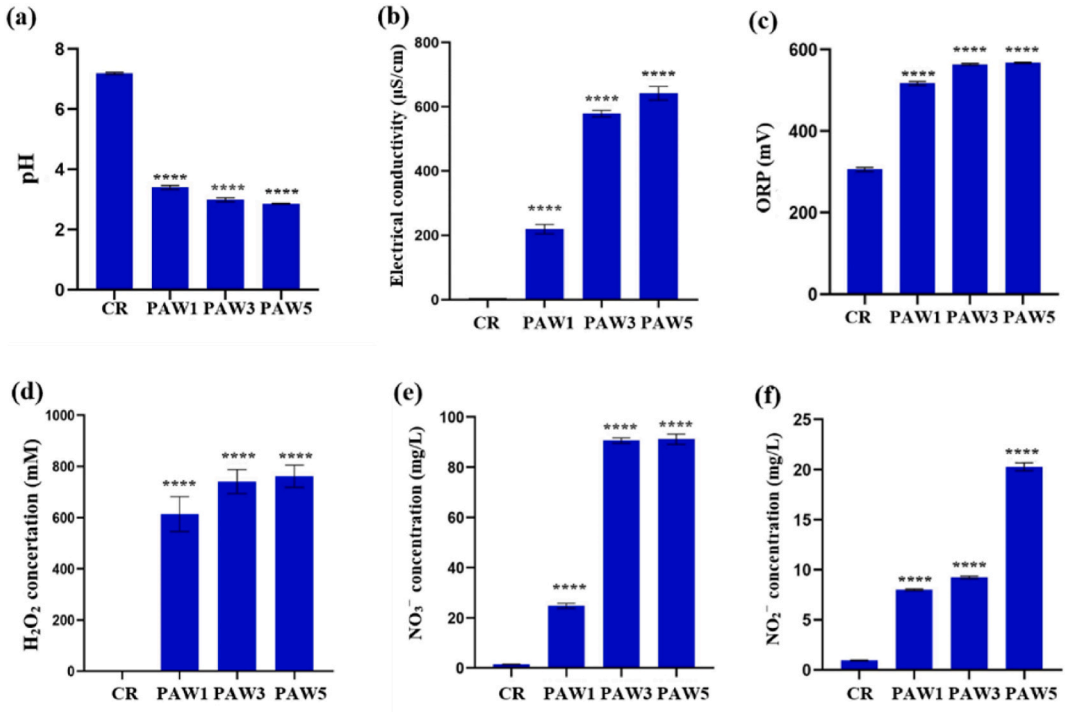

Fig. 4. Changes in the pH (a), electrical conductivity (b), ORP (c), H_2O_2 (d), NO_3^- (e) and NO_2^- (f) concentration of PAW over 5 min of CAP irradiation. "****" indicates extremely significant difference as compared with the CR group ($P < 0.0001$).

of PAW significantly increased from 4.92 (±0.09) μS/cm to 641.67 (21.01) μS/cm, and from 306.00 (±4.58) mV to 567.67 (±1.53) mV, respectively. Fig. 4d, e and 4f illustrate the generation of H_2O_2, NO_3^-, and NO_2^- in PAW treated with CAP; their concentration rose to 873.02 (±19.92) mmol/L, 1.405 (±0.007) μmol/mL, and 0.095 (±0.002) μmol/mL in 5 min, respectively.

3.4. The major sterile effector of PAW

To confirm the primary sterile effector of PAW, the Pearson's correlations between physicochemical parameters and the antiviral efficiency of PAW1, PAW3, and PAW5 were evaluated. The Pearson correlation coefficients for the antiviral efficiency in relation to H_2O_2, NO_3^-, and NO_2^- concentrations were found to be 0.639, 0.892, and 0.942, respectively. Therefore, significantly positive correlation was obtained between antiviral efficiency of PAW and H_2O_2, NO_3^-, as well as NO_2^- concentration. To evaluate the effect of these long-lived species in PAW, a mixture of H_2O_2 (873 mmol/L), NO_3^- (1.405 μmol/mL), and NO_2^- (0.095 μmol/mL) was used to treat the pseudovirus. However, this treatment inactivated the pseudovirus only by 6.29 % (±0.69 %), indicating that the three long-living species are not the major sterile effectors. Therefore, it was necessary to investigate whether the short-living ROS species, including hydroxyl radicals(•OH), singlet oxygen ($^1O_2$), and peroxynitrite ($ONOO^-$), could act as the major sterile effectors of PAW. In this study, the common RONS scavengers, which were superoxide dismutase mimetic Mn(III)tetrakis (4-benzoic acid) porphyrin (MnTBAP) for peroxynitrite, and *N*-acetyl-L-cysteine (NAC) for ROS were used to distinguish the contribution of the different short-living species to the viricidal effect of PAW5. We established that MnTBAP reduced the antiviral efficiency of PAW5 on the pseudovirus to 4.24 % (±0.97 %), whereas NAC only reduced the antiviral efficiency of PAW5 on the pseudovirus to 85.85 % (±0.72 %). These data suggested that ONOO- significantly contributed to the inactivation effect of PAW against the pseudovirus. Next, to determine the effect of pH on the virucidal ability, pH of PAW5 was adjusted to 7.0, and its antiviral efficiency was detected. The results showed that the antiviral efficiency was significantly decreased from 91.71 % (±0.47 %) to 21.71 % (±1.02 %).

3.5. Lipid peroxidation of the pseudoviral envelope

Lipid peroxidation of the pseudoviral envelope can result in destruction of the pseudovirus. MDA, one of the most common by-products of lipid peroxidation, is frequently used as a biomarker for lipid peroxidation. The graph in Fig. 5 depicts the calibrated concentration of MDA in the pseudovirus in the different treatment groups. The calibrated MDA concentration was 0 in the pseudovirus treated with PAW1, which was the same as that treated with CR. As expected, the calibrated MDA concentration of pseudovirus on the swine skin treated with PAW3 and PAW5 increased significantly from 0 to 5.94 (±0.23) μM and to 6.59 (±0.79) μM, respectively.

3.6. Effects of PAW on the RBD protein of the pseudovirus

Altering the binding ability of the RBD region is one of the possible mechanisms of SARS-CoV2 pseudovirus infection prevention by PAW [17]. Thus, we treated the RBD sample with different PAW exposure doses to assess whether cleavage of the peptide chain was induced. SDS-PAGE analysis was performed followed by silver staining. As can be seen in Fig. 6a, the RBD protein on the swine skin treated by PAW displayed obvious brands between 30 and 37 kDa in their lanes, which had the same location, brightness and thickness as that of the control group. The results of SDS-PAGE indicated that the RBD protein on the swine skin was not degraded by PAW.

Further, an ELISA experiment was conducted to verify the effect of PAW on RBD protein binding activity. The A_{450nm} values of the RBD protein in the CR, PAW1, PAW3, and PAW5 treatments were 0.78 (±0.02), 0.79 (±0.03), 0.75 (±0.03), and 0.75 (±0.05), respectively, with no significant differences (Fig. 6b). These results confirmed that the binding activity of the RBD protein on swine skin was not changed by PAW.

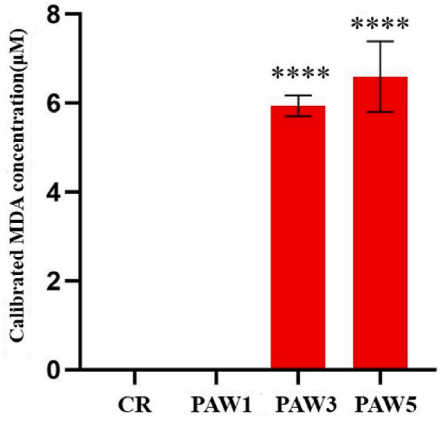

Fig. 5. Calibrated MDA concentration of the pseudovirus treated with CR and PAWs. "****" indicates extremely significant difference as compared with the CR group ($P < 0.0001$).

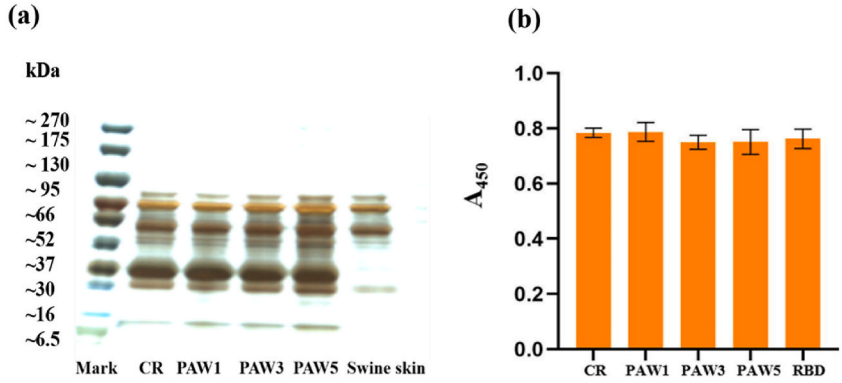

Fig. 6. SDS-PAGE image (a) and ELISA results (b) of the spike RBD protein treated with CR and PAWs. (a) To eliminate the interference caused by the protein existing on the swine skin, the PBS eluent of the swine skin was loaded into one of the electric lanes of SDS-PAGE, which is marked as "swine skin" on the image; (b) "RBD" represents original the RBD solution which had not been added on the swine skin; this group was set to eliminate the effect of swine skin on RBD.

3.7. Effects of PAW on RNA of pseudovirus

It is of importance to confirm whether pseudoviral RNA was also a target of PAW with a role in viral inactivation on the swine skin. Thus, we evaluated the effects of PAW on pseudoviral RNA by qPCR. As can be observed in Fig. 7, the RNA reduction in the pseudovirus treated with CR was set as 0, and then the RNA reduction of pseudovirus treated with PAW1, PAW3, and PAW5 were 2.1 % (±0.3 %), 16.69 % (±4.4 %), and 23.37 % (±2.26 %), respectively. Based on this experimental evidence, we suggest that both PAW3 and PAW5 significantly but not completely degraded the pseudoviral RNA on the swine skin.

3.8. No cytotoxicity of PAW to the normal skin cells

CCK8 assay was conducted to determine the cytotoxic effect of PAW5 on normal skin cells. As visible in Fig. 8, in HaCaT cells (normal skin cells) treated with PAW, the viability was nearly equal to that of the control cells. Based on the results of the cytotoxicity assay, PAW had no toxicity to normal skin cells.

4. Discussion

Previous research has evidenced the potential of PAW as a novel disinfectant due to its outstanding inactivation effect against a broad range of pathogens, including *S. aureus* [27], *E. coli* [28], and Newcastle disease virus [16b]. Additionally, several studies have highlighted the mechanisms underlying microbial inactivation by PAW, which involve interactions between PAW's reactive species and the structural components of bacteria or viruses. These interactions result in processes such as lipid peroxidation, protein degradation, and nucleic acid damage [29]. Importantly, PAW is free from harmful chemicals and non-toxic to normal skin cells [14, 30]. Therefore, it is worth investigating whether PAW can be utilized as an effective hand disinfectant to mitigate self-inoculation of

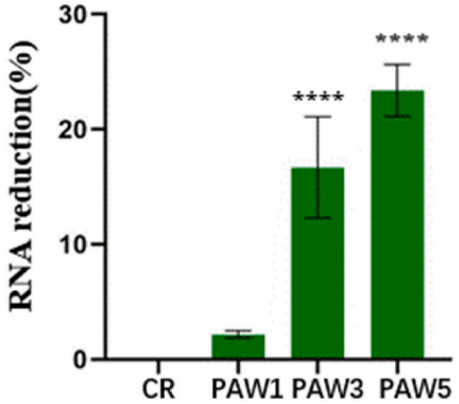

Fig. .7. RNA reduction of pseudovirus treated with CR and PAWs. "****" indicates extremely significant difference as compared with the CR group ($P < 0.0001$).

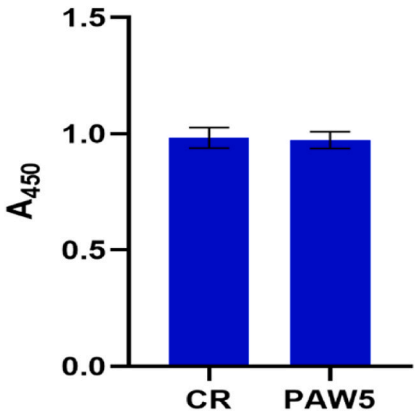

Fig. .8. Cytotoxicity of PAW5 to HaCaT cells. Cell viability was investigated by CCK8 assay after treatment with PAW5 and CR. As a result, the A_{450} of HaCaT cells treated with PAW5 and CR were 0.98 (0.04) and 0.97 (0.04), respectively.

SARS-CoV-2.

Lee et al. demonstrated the effectiveness of PAW as a skin disinfectant against SARS-CoV-2 [30]. However, their study was limited to an infected cell solution. In our research, PAW1 showed no inactivation effect on the SARS-CoV-2 pseudovirus on swine skin, while PAW3 significantly inactivated the pseudovirus. Furthermore, PAW5 completely inactivated the pseudovirus on swine skin. These results confirm the dose-dependent inactivation effect of PAW on SARS-CoV-2 on swine skin.

The potential of both CAP and PAW to destroy the structure of the feline calicivirus [31] and T4 bacteriophage [16a] has been confirmed. Additionally, PAW was reported to cause cell membrane leakage through the oxidative stress which allowed the RONS to enter the cells [32]. In our study, PAW3 may have caused leakage of the pseudovirus envelope, enabling PAW-inherent RONS to enter and inactivate the pseudovirus. Complete structural collapse of the pseudovirus was observed with PAW5, which explains its thorough inactivation effect on the pseudovirus on swine skin. Thus, the destruction of the pseudoviral structure by PAW is the crucial mechanism underlying its virucidal effect.

The CAP exposure dose of PAW is a crucial factor in its viral inhibition effect [16a]. However, the reference value of the exposure dose is limited due to variations in CAP devices and operating parameters used in different studies. To address this issue, the physicochemical properties of PAW, such as pH, electrical conductivity, ORP, H_2O_2, and NO_3^- and NO_2^- concentration, have been used as general and rapidly established indexes to investigate the antimicrobial mechanisms of PAW and expand its potential applications [13b]. PAW has a lower pH value but higher electrical conductivity and ORP compared to ultrapure water. The generation of ions, including H^+, NO_3^-, and NO_2^-, decreases pH and increases the electrical conductivity of PAW [33]. Meanwhile, mainly the formation of H_2O_2 in PAW is regarded to be responsible for the enhancement of its ORP [34].

In our experiment, both acidification (pH decrease from 7.19 to 3.40) and the increase of H_2O_2 concentration observed in PAW1, which had a weak deactivation effect on the pseudovirus. Thus, neither acidic pH nor H_2O_2 concentration of PAW was confirmed to be the dominant parameter inducing its antiviral effect. Similar results were also obtained by Tian et al. [35], who found that the higher disinfection efficiency of PAW against *S. aureus* was not associated with the pH value and H_2O_2 concentration. Nevertheless, the experimental results presented here indicated that at non-acidic pH, PAW loses most of its antiviral ability. Additionally, the pH values of PAW3 and PAW5, which both inactivated the pseudovirus, were significantly lower than that of PAW1. Basically, two main mechanisms of the antimicrobial activity-inducing effects of acidic pH on on PAW. On the one hand, as Gaunt et al. proposed, a PAW-generated superoxide radical accepts a proton in acidic environment proceeding to form a hydroperoxyl radical, which penetrates the lipid membrane and then changes to hydroxyl radical in the cytosol (pH = 7.2) resulting in devast of cellular structure [36]. On the other hand, the formation of NO_2^- and H_2O_2 in PAW under acidic environment may proceed to form the peroxynitrite (ONOOH) through the reaction $NO_2^- + H_2O_2 + H^+ \rightarrow ONOOH + H_2O$ [29a].

Peroxynitrite is an isomer of NO_3^-, which has been recognized as the major sterile effector of PAW [13a,37]. For example, Hye Ran Lee et al. reported that peroxynitrite significantly contributed bactericidal effect of PAW against *S. aureus* [30]. Another example, Li Guo et al. suggests that peroxynitrite in PAW play crucial roles in the inactivation against SARS-COV-2. However, the half-life of peroxynitrite is less than 1s, which is too short to explain the anti-microbial effect of PAW. Therefore, it is of great necessity to continuously generate the peroxynitrite in PAW through the synergism of acidic environment, NO_2^- and H_2O_2. The short-living species in PAW, including peroxynitrite, singlet oxygen, and •OH radical, easily react with a wide range of organic compounds [38]. Therefore, the various self-contained compounds on the surface of swine skin may weaken the effect of these short-living species in PAW [24]. We speculated that no sufficient peroxynitrite was formed in PAW1 to counteract the interference of the impurities on the swine skin, because of its higher pH value and lower concentration of NO_2^- than those of PAW3 and PAW5. All in all, our experimental results suggested that peroxynitrite was identified as the major sterile effector of PAW, and acidic environment, NO_2^- and H_2O_2 were prerequisites for the formation of peroxynitrite.

Peroxynitrite in PAW is known to cause lipid peroxidation of microbial membranes [32,39]. The lipid envelope of SARS-CoV-2 contains polyunsaturated fatty acids, which are susceptible to peroxidation by peroxynitrite [40]. The resulting levels of

malondialdehyde (MDA), a marker of lipid peroxidation, were significantly higher in the pseudovirus treated with PAW3 and PAW5 compared to the control. However, the MDA levels in the pseudovirus treated with PAW3 and PAW5 were similar, despite differences in the antiviral activity assay and TEM observations. This suggests that PAW may have additional anti-SARS-CoV-2 mechanisms on swine skin. Dolezalova and Lukes [41] also reported an increased MDA level of *E. coli* under prolonged PAW treatment, indicating lipid peroxidation of the microbial membrane. However, the MDA levels of the pseudovirus treated with PAW3 and PAW5 were similar, which differed from the results of the antiviral activity assay and TEM observations. Thus, other anti-SARS-COV-2 mechanisms are possible to have been realized by PAW on the swine skin.

Prior research has shown that peroxynitrite in PAW can degrade viral proteins, contributing to its inactivation effect on SARS-CoV-2 [17]. Interestingly, the NO_2^- level in PAW5 was more than twice that of PAW3 under more acidic conditions, potentially resulting in a higher peroxynitrite content. However, our results indicate that PAW had little effect on the receptor-binding domain (RBD) protein of SARS-CoV-2. Considering that the RBD protein is only a fragment of the S-protein, the degradation of the S-protein may be another mechanism leading to viral destruction on swine skin, requiring further investigation for confirmation.

RONS in PAW can attack the sugar-phosphate backbone of viral DNA/RNA, subsequently leading to viral death [16,42]. As expected, the increasing trend of RNA reduction was consistent with that of PAW's inhibitory effect on the pseudovirus. However, the pseudovirus RNA reduction caused by treatment with PAW5 was only around 23.37 %, whereas complete pseudovirus inactivation was achieved in the PAW5 treatment. Therefore, the degradation of the viral RNA by PAW is probably one of the important SARS-COV-2 inactivation mechanisms.

5. Conclusion

In conclusion, the findings of this study demonstrate the ability of PAW to deactivate the SARS-CoV-2 pseudovirus on swine skin. This suggests that PAW has the potential to serve as an effective hand disinfectant for preventing self-inoculation of SARS-CoV-2. The proposed mechanism of PAW-induced SARS-CoV-2 inactivation involves the generation of peroxynitrite through the synergistic effects of an acidic environment and reactive species. This peroxynitrite formation may lead to changes in viral morphology and degradation of viral RNA. Further investigations are needed to elucidate the interaction mechanism between PAW's inherent reactive oxygen and nitrogen species (RONS) and viral components.

Ethics approval

No permissions were required prior to conducting field studies.

Funding

This research was funded by Key Research Project of Anhui Provincial Health Commission in 2022 (AHWJ2022a006), Key Laboratory Construction Project for Medicine and Health of Anhui Province (grant number 93), the National Special Project for Magnetic Confinement Nuclear Fusion Energy Development (2022YFE03080000), Key programs of the Scientific Research Program of Higher Education Institutions of Anhui Province in 2023 (No.: 2023AH052601; No.: 2023AH052602), Collaborative Innovation Program of Hefei Science Center (CAS, CX2140000018), and the Funding for Joint Lab of Applied Plasma Technology (JL06120001H).

Consent to participate

Not applicable.

Consent to publish

Not applicable.

Data availability statement

Data will be made available on request.

CRediT authorship contribution statement

Yong Xu: Writing – original draft, Methodology, Investigation, Data curation. **Tao Jin:** Writing – original draft, Investigation. **Yu Bai:** Writing – review & editing. **Xiuhong Zhou:** Writing – original draft. **Han Lv:** Writing – original draft. **Chenwei Dai:** Investigation, Funding acquisition. **Zhengwei Wu:** Writing – review & editing, Funding acquisition, Conceptualization. **Qinghua Xu:** Writing – review & editing, Funding acquisition, Conceptualization.

Declaration of competing interest

The authors declare no financial or commercial conflict of interest.

References

[1] C.A. Tisdell, Economic, social and political issues raised by the COVID-19 pandemic, Econ. Anal. Pol. 68 (2020) 17–28.
[2] M. Rebeaud, F. Zores, SARS-CoV-2 and the Use of chloroquine as an antiviral treatment, Front. Med. 7 (2020).
[3] M.Y. Wang, R. Zhao, L.J. Gao, X.F. Gao, D.P. Wang, J.M. Cao, SARS-CoV-2: structure, biology, and structure-based therapeutics development, Front. Cell. Infect. Microbiol. 10 (2020) 587269.
[4] Y. Huang, C. Yang, X.F. Xu, W. Xu, S.W. Liu, Structural and functional properties of SARS-CoV-2 spike protein: potential antivirus drug development for COVID-19, Acta Pharmacol. Sin. 41 (9) (2020) 1141–1149.
[5] a) L. Xie, F. Liu, J. Liu, H. Zeng, A nanomechanical study on deciphering the stickiness of SARS-CoV-2 on inanimate surfaces, ACS Appl. Mater. Interfaces 12 (52) (2020) 58360–58368;
b) D.E. Harbourt, A.D. Haddow, A.E. Piper, H. Bloomfield, B.J. Kearney, D. Fetterer, K. Gibson, T. Minogue, Modeling the stability of severe acute respiratory syndrome coronavirus 2 (SARS-CoV-2) on skin, currency, and clothing, PLoS Neglected Trop. Dis. 14 (11) (2020) e0008831.
[6] Y. Kwok, J. Gralton, M.L. McLaws, Face touching: a frequent habit that has implications for hand hygiene, Am. J. Infect. Control 43 (2015) 112–114.
[7] M. Nicas, D. Best, A study quantifying the hand-to-face contact rate and its potential application to predicting respiratory tract infection, J. Occup. Environ. Hyg. 5 (6) (2008) 347–352.
[8] a) E. Hoseinzadeh, J. Safoura, M. Farzadkia, F. Mohammadi, H. Hossini, M. Taghavi, An updated min-review on environmental route of the SARS-CoV-2 transmission, Ecotoxicol. Environ. Saf. 202 (2020) 111015;
b) H. Kanamori, Rethinking environmental contamination and fomite transmission of SARS-CoV-2 in the healthcare, J. Infect. 82 (1) (2021) e17–e18.
[9] a) S.A. Mir, M.A. Shah, M.M. Mir, Understanding the role of plasma technology in food industry, Food Bioprocess Technol. 9 (5) (2016) 1–17;
b) A.I. Muhammad, Q. Xiang, X. Liao, D. Liu, D. Tian, Understanding the impact of nonthermal plasma on food constituents and microstructure—a review, Food Bioprocess Technol. 11 (3) (2018) 463–486.
[10] X. Zhang, R. Zhou, K. Bazaka, Y. Liu, R. Zhou, G. Chen, Z. Chen, Q. Liu, S. Yang, K. Ostrikov, Quantification of plasma produced OH radical density for water sterilization, Plasma Process. Polym. 15 (2018) 1700241.
[11] Z. Chen, G. Garcia Jr., V. Arumugaswami, R.E. Wirz, Cold atmospheric plasma for SARS-CoV-2 inactivation, Phys. Fluids 32 (11) (2020) 111702.
[12] T. Jin, Y. Xu, C. Dai, X. Zhou, Q. Xu, Z. Wu, Cold atmospheric plasma: a non-negligible strategy for viral RNA inactivation to prevent SARS-CoV-2 environmental transmission, AIP Adv. 11 (8) (2021) 085019.
[13] a) S. Herianto, C. Hou, C. Lin, H. Chen, Nonthermal plasma-activated water: a comprehensive review of this new tool for enhanced food safety and quality, Compr. Rev. Food Sci. Food Saf. 20 (1) (2021) 583–626;
b) Y.M. Zhao, A. Patange, D.W. Sun, B. Tiwari, Plasma-activated water: physicochemical properties, microbial inactivation mechanisms, factors influencing antimicrobial effectiveness, and applications in the food industry, Compr. Rev. Food Sci. Food Saf. 19 (6) (2020) 3951–3979.
[14] R. Zhou, R. Zhou, P. Wang, Y. Xian, K. Bazaka, Plasma activated water (PAW): generation, origin of reactive species and biological applications, J. Phys. D Appl. Phys. 53 (30) (2020) 303001.
[15] T.P. Chen, J. Liang, T.L. Su, Plasma-activated water: antibacterial activity and artifacts? Environ. Sci. Pollut. Res. Int. 25 (27) (2018) 26699–26706.
[16] a) L. Guo, R. Xu, L. Gou, Z. Liu, Y. Zhao, D. Liu, L. Zhang, H. Chen, M.G. Kong, Mechanism of virus inactivation by cold atmospheric-pressure plasma and plasma-activated water, Appl. Environ. Microbiol. 84 (17) (2018) e00726, 00718;
b) X. Su, Y. Tian, H. Zhou, Y. Li, Z. Zhang, B. Jiang, B. Yang, J. Zhang, J. Fang, Inactivation efficacy of nonthermal plasma-activated solutions against Newcastle disease virus, Appl. Environ. Microbiol. 84 (9) (2018) e02836, 02817.
[17] L. Guo, Z. Yao, L. Yang, H. Zhang, Y. Qi, L. Gou, W. Xi, D. Liu, L. Zhang, Y. Cheng, X. Wang, M. Rong, H. Chen, M.G. Kong, Plasma-activated water: an alternative disinfectant for S protein inactivation to prevent SARS-CoV-2 infection, Chem. Eng. J. 421 (2021) 127742.
[18] C. Tan, C. Gao, Q. Zhou, W. Van Driel, H. Ye, G. Zhang, The inactivation mechanism of chemical disinfection against SARS-CoV-2: from MD and DFT perspectives, RSC Adv. 10 (66) (2020) 40480–40488.
[19] B. Lange-Asschenfeldt, A. Alborova, D. Kruger-Corcoran, A. Patzelt, H. Richter, W. Sterry, A. Kramer, E. Stockfleth, J. Lademann, Effects of a topically applied wound ointment on epidermal wound healing studied by in vivo fluorescence laser scanning microscopy analysis, J. Biomed. Opt. 14 (5) (2009) 054001.
[20] O. Lademann, A. Kramer, H. Richter, A. Patzelt, M.C. Meinke, V. Czaika, K.D. Weltmann, B. Hartmann, S. Koch, Skin disinfection by plasma-tissue interaction: comparison of the effectivity of tissue-tolerable plasma and a standard antiseptic, Skin Pharmacol. Physiol. 24 (5) (2011) 284–288.
[21] T. Royintarat, E.H. Choi, D. Boonyawan, P. Seesuriyachan, W. Wattanutchariya, Chemical-free and synergistic interaction of ultrasound combined with plasma-activated water (PAW) to enhance microbial inactivation in chicken meat and skin, Sci. Rep. 10 (1) (2020) 1559.
[22] U. Schubert, A colorimetric method for the determination of nitrate in urine, Z. Med. Labdiagn. 31 (8) (1990) 454–455.
[23] T. Parsons, Y. Maita, C. Lalli, in: Determination of Nitrite, 1984, pp. 7–9.
[24] L. Rosenberg, C. Bagger, C. Janfelt, M. Haedersdal, U. Olesen, C. Lerche, A comparison of human and porcine skin in laser-assisted drug delivery of chemotherapeutics, Laser Surg. Med. 53 (2020).
[25] F. Capelli, S. Tappi, T. Gritti, A.C. Pinheiro, S. Pinheiro, R. Laurita, U. Tylewicz, F. Spataro, G. Braschi, R. Lanciotti, F. Galindo, V. Siracusa, S. Romani, M. Gherardi, V. Colombo, V. Sambri, P. Rocculi, Decontamination of food packages from SARS-COV-2 RNA with a cold plasma-assisted system, Appl. Sci. 11 (2021) 4177.
[26] C.M. Lin, C.P. Hsiao, H.S. Lin, J.S. Liou, C.W. Hsieh, J.S. Wu, C.Y. Hou, The antibacterial efficacy and mechanism of plasma-activated water against Salmonella enteritidis (ATCC 13076) on shell eggs, Foods 9 (10) (2020).
[27] V.S.S.K. Kondeti, C. Phan, K. Wende, H. Jablonowski, U. Gangal, J. Granick, R. Hunter, P. Bruggeman, Long-lived and short-lived reactive species produced by a cold atmospheric pressure plasma jet for the inactivation of Pseudomonas aeruginosa and Staphylococcus aureus, Free Radic. Biol. Med. 124 (2018).
[28] S. Ikawa, A. Tani, Y. Nakashima, K. Kitano, Physicochemical properties of bactericidal plasma-treated water, J. Phys. Appl. Phys. 49 (42) (2016) 425401.
[29] a) P. Lukes, E. Dolezalova, I. Sisrova, M. Clupek, Aqueous-phase chemistry and bactericidal effects from an air discharge plasma in contact with water: evidence for the formation of peroxynitrite through a pseudo-second-order post-discharge reaction of H2O 2 and HNO2, Plasma Sources Sci. Technol. 23 (2014) 015019;
b) A. Mai-Prochnow, M. Clauson, J. Hong, A. Murphy, Gram positive and Gram negative bacteria differ in their sensitivity to cold plasma, Sci. Rep. 6 (2016) 38610.
[30] H.R. Lee, Y.S. Lee, Y.S. You, J.Y. Huh, K. Kim, Y.C. Hong, C.H. Kim, Antimicrobial effects of microwave plasma-activated water with skin protective effect for novel disinfectants in pandemic era, Sci. Rep. 12 (1) (2022) 5968.
[31] H.A. Aboubakr, S.K. Mor, L. Higgins, A. Armien, M.M. Youssef, P.J. Bruggeman, S.M. Goyal, Cold argon-oxygen plasma species oxidize and disintegrate capsid protein of feline calicivirus, PLoS One 13 (3) (2018) e0194618.
[32] S.G. Joshi, M. Cooper, A. Yost, M. Paff, U.K. Ercan, G. Fridman, G. Friedman, A. Fridman, A.D. Brooks, Nonthermal dielectric-barrier discharge plasma-induced inactivation involves oxidative DNA damage and membrane lipid peroxidation in Escherichia coli, Antimicrob. Agents Chemother. 55 (3) (2011) 1053–1062.
[33] J.-L. Brisset, B. Benstaali, D. Moussa, J. Fanmoe, E. Njoyim-Tamungang, Acidity control of plasma-chemical oxidation: applications to dye removal, urban waste abatement and microbial inactivation, Plasma Sources Sci. Technol. 20 (2011) 034021.
[34] P. Lukes, B. Locke, J.-L. Brisset, In *Aqueous-phase Chemistry Of Electrical Discharge Plasma in Water and in Gas-Liquid Environments*, 2012, pp. 243–308.
[35] Y. Tian, R. Ma, Q. Zhang, H. Feng, Y. Liang, J. Zhang, J. Fang, Assessment of the physicochemical properties and biological effects of water activated by non-thermal plasma above and beneath the water surface: physicochemical and biological properties of PAW, Plasma Process. Polym. 12 (2014).
[36] L. Gaunt, C. Beggs, G. Georghiou, Bactericidal action of the reactive species produced by gas-discharge nonthermal plasma at atmospheric pressure: a review, Plasma Science, IEEE Transactions on 34 (2006) 1257–1269.
[37] J.-L. Brisset, H. Eugen, Peroxynitrite: a Re-examination of the chemical properties of non-thermal discharges burning in air over aqueous solutions, Plasma Chem. Plasma Process. 32 (2012).

[38] F. Wilkinson, W. Helman, A. Ross, Rate constants for the decay and reactions of the lowest electronically excited singlet state of molecular oxygen in solution. An expanded and revised compilation, J. Phys. Chem. Ref. Data 24 (1995) 663–1021.
[39] R. Zhou, K. Prasad, Z. Fang, R. Speight, K. Bazaka, K. Ostrikov, Cold atmospheric plasma activated water as a prospective disinfectant: the crucial role of peroxynitrite, Green Chem. 20 (2019).
[40] E. Dolezalova, P. Lukes, Membrane damage and active but nonculturable state in liquid cultures of Escherichia coli treated with an atmospheric pressure plasma jet, Bioelectrochemistry 103 (2015) 7–14.
[41] E. Dolezalova, P. Lukes, Membrane damage and active but nonculturable state in liquid cultures of Escherichia coli treated with an atmospheric pressure plasma jet, Bioelectrochemistry (2014) 103.
[42] R. Zhou, R. Zhou, X. Zhang, J. Zhuang, S.-Z. Yang, K. Bazaka, K. Ostrikov, Effects of atmospheric-pressure N2, He, air, and O2 microplasmas on mung bean seed germination and seedling growth, Sci. Rep. 6 (2016) 32603.